Supporting Information for

Molecular insights into the potential and temperature dependence of the differential capacitance of a room temperature ionic liquid at graphite electrodes

Jenel Vatamanu, Oleg Borodin and Grant D. Smith

Department of Materials Science and Engineering, University of Utah, Salt Lake City, UT 84112

Snapshot of the Simulated Ionic Liquid Sandwiched Between Graphite Electrodes

A representative snapshot of [pyr_{13}][TFSI] sandwiched between graphite electrodes is shown in Figure S1.

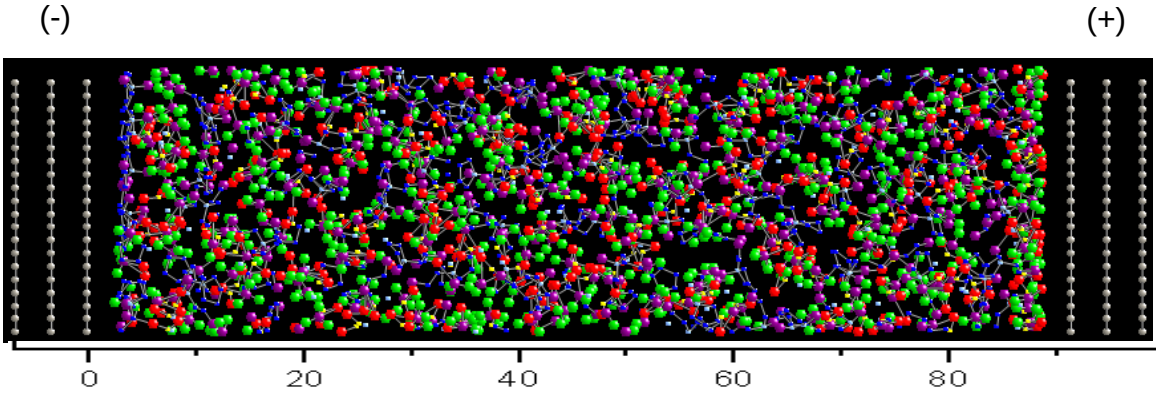

Figure S1. A snapshot of a typical simulation setup at 4.3 V potential between electrodes at 393 K for a 2D-geometry system. The electrode atoms are represented as grey spheres. The (-) and (+) sign indicate the polarity of the electrodes. The scale at the bottom of the figure indicates the distances along the direction normal to electrode surface (our OZ axes). [pyr_{13}][TFSI] colors correspond to the colors shown in Figure 1 of the manuscript.

The Electrode Potential and Differential Capacitance

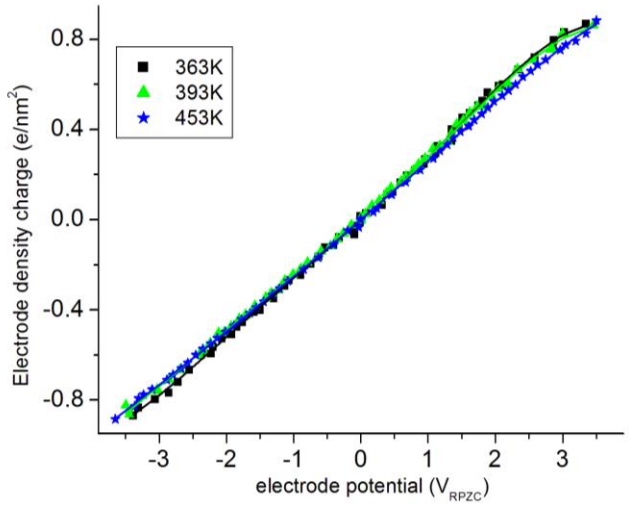

Figure S2. Surface charges vs. electrode potential from MD simulations. The symbols are simulation results while the solid lines are polynomial fits to simulation data.

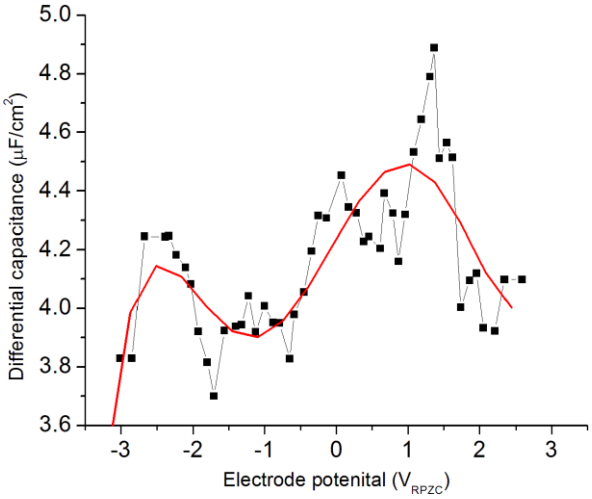

Figure S3. The differential capacitance (DC) obtained from local fit to electrode charges vs. potential using 2nd order polynomial over 9 consecutive points (which correspond to electrode potential widths between 0.6V-1V). The differential capacitance was evaluated in the middle point as the analytical derivative of the fitted parabola. The solid squares are the differential capacitance points from MD simulations obtained from such local fit. The red line corresponds to the DC from the order 5 polynomial fit over the whole potential range as discussed in Section **Differential Capacitance** of the manuscript. We conclude that the DC from the local fit (using 2nd order polynomial) is in qualitative agreement with the DC derived from the global fit using order five polynomial.

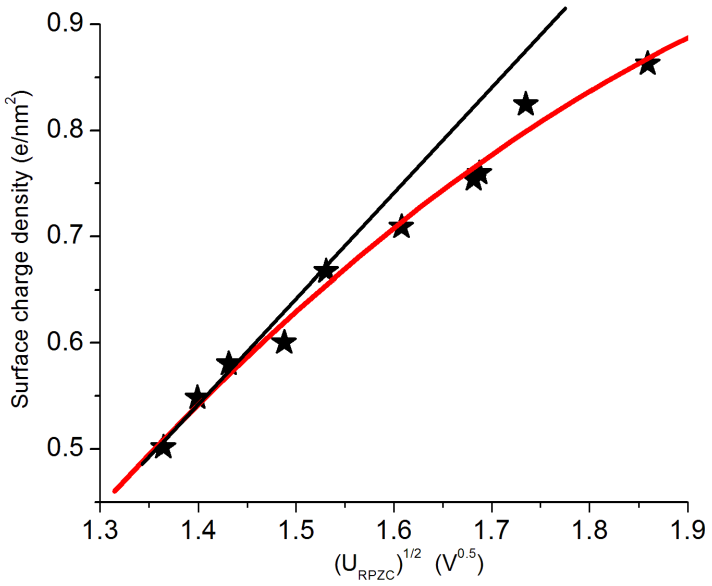

Figure S4. Electrode charge vs. the square-root of electrode potential. The star symbols are simulation data points, the red line is the fit to MD data.

The MD simulation data show that the surface charge decays faster than the linear behavior expected for $C \propto |U|^{-0.5}$,thus, indicating that for this potential range the exponent for the limiting behavior is higher (in magnitude) than -0.5. In fact, the exponent was found to be around -0.73 for the local fit shown in Figure S4.

Development of the United Atom Force Field

A nonpolarizable united atom (UA) force field for *N*-methyl-*N*-propylpyrrolidinium (pyr_{13}^+) bis(trifluoromethane) sulfonamide ($TFSI^-$) has been developed using all atom (AA) APPLE&P (Atomistic Polarizable Potential for Liquids, Electrolytes and Polymers)[1] as a starting point. In the process of UA force field development for [pyr_{13}][TFSI] we also developed a nonpolarizable UA force fields for n-alkanes (validating it for C_5H_{12}, $C_{10}H_{22}$) and two other ionic liquids [*N*-methyl-*N*-butylpyrrolidinium (pyr_{14}^+)][$TFSI^-$] and [$(CH_3)_3N^+(C_4H_9)$][TFSI] denoted as [N_{4111}][TFSI]. These additional compounds (n-alkanes and [N_{4111}][TFSI]) were needed to derive the non-bonded repulsion-dispersion parameters for [pyr_{13}][TFSI], while [pyr_{14}][TFSI] was used perform an additional force field validation. Specifically, the terminal methyl group and ethylene carbon repulsion-dispersion parameters were derived from n-alkane density and heat of vaporization, while the repulsion-dispersion parameters for the terminal methyl group attached to the N^+ in ionic liquid (IL) cations were largely based on the density, heat of vaporization and ion self-diffusion coefficients of [N_{4111}][TFSI] as discussed below.

As in APPLE&P the potential energy $U^{tot}(\mathbf{r})$ to atomic coordinates **r** for the ensemble of atoms was split into non-bonded $U^{NB}(\mathbf{r})$ and bonded contributions as given by,

$$U^{tot}(\mathbf{r}) = U^{NB}(\mathbf{r}) + \sum_{bends} U^{BEND}(\theta_{ijk}) + \sum_{dihedrals} U^{DIHEDRAL}(\phi_{ijkl}) + \sum_{\substack{improper \\ dihedrals}} U^{IMP}(\phi_{ijkl}^{imp}), \quad (1)$$

where the sums are over all bonds, bends, dihedrals and improper dihedrals in the system. The contributions to the potential energy due to bonds, bends, dihedrals and out-of-plane bending (improper dihedrals) are

$$U^{BEND}(\theta_{ijk}) = \frac{1}{2} k_{\alpha\beta\gamma}^{BEND}(\theta_{ijk} - \theta_{ijk}^{0})^2 \quad (2)$$

$$U^{DIHEDRAL}(\phi_{ijkl}) = \sum_{n} \frac{1}{2} k_{\alpha\beta\gamma\delta,n}^{DIHEDRAL}[1 - \cos(n\phi_{ijkl})] \quad (3)$$

$$U^{IMP}(\phi_{ijkl}^{imp}) = \tfrac{1}{2} k_{\alpha\beta\gamma\delta}^{IMP}(\phi_{ijkl}^{imp})^2 \quad (4)$$

where θ_{ijk} and θ_{ijk}^{0} are the instantaneous and natural bending angles for atoms *i*, *j* and *k*; ϕ_{ijkl} is the dihedral angle for atoms *i*, *j*, *k* and *l*; and ϕ_{ijkl}^{imp} is the out-of-plane bending angle for an sp^2 center at atom *j* that will be used in future simulations with imidazolium cations. The strength of these interactions is characterized by the corresponding force constants $k_{\alpha\beta\gamma}^{BEND}$, $k_{\alpha\beta\gamma\delta,n}^{DIHEDRAL}$, and $k_{\alpha\beta\gamma\delta}^{IMP}$, respectively. The subscripts α, β, γ, and δ denote atom type for atoms *i*, *j*, *k*, and *l*, respectively.

The nonbonded energy $U^{NB}(\mathbf{r})$ consists of the sum of two-body repulsion and dispersion energy terms $U^{RD}(\mathbf{r})$, the energy due to interactions of fixed charges $U^{coul}(\mathbf{r})$,

$$U^{NB}(\mathbf{r}) = U^{RD}(\mathbf{r}) + U^{coul}(\mathbf{r})) = \sum_{i>j} \left(A_{\alpha\beta} \exp(-B_{\alpha\beta} r_{ij}) - C_{\alpha\beta} r_{ij}^{-6} + D\left(\frac{12}{B_{\alpha\beta} r_{ij}}\right)^{12} \right) + \sum_{i>j} \left(\frac{q_i q_j}{4\pi\varepsilon_0 r_{ij}} \right). \quad (5)$$

where $A_{\alpha\beta}$ and $B_{\alpha\beta}$ are the repulsion parameters and $C_{\alpha\beta}$ is the dispersion parameter for interaction between atoms *i* and *j* with atom types α and β. The term $D\left(\frac{12}{B_{\alpha\beta} r_{ij}}\right)^{12}$, with $D = 5 \cdot 10^{-5}$ kcal/mol for all pair interactions, is essentially zero at typical nonbonded atomic separations, but becomes the dominant term at $r_{ij} < 1$ Å, ensuring that $U^{RD}(\mathbf{r})$ is repulsive at distances much smaller than the size of an atom. Intramolecular nonbonded interactions are included for atoms separated by three or more covalent bonds. The intramolecular interaction between an induced dipole and a partial charge separated by 3 bonds was scaled by 0.8. Finally, for heteroatom interactions, the modified Waldman-Hagler combining rules[2] were used

$$A_{ij} = \sqrt{A_{ii}A_{jj}}\,\frac{B_{ij}^{\,6}}{B_{ii}^{\,3}B_{jj}^{\,3}}; B_{ij} = \left(\frac{2}{B_{ii}^{\,-6} + B_{jj}^{\,-6}}\right)^{1/6}; C_{ij} = \sqrt{C_{ii}C_{jj}}\,. \qquad (6)$$

These combining rules have been successfully used by us for simulations of liquids,[2-3] polymers, electrolytes[2, 4] and ionic liquids.[5]

The force field parameterization proceeded in the following way. First, partial charges for $TFSI^-$, N_{4111}^+ and pyr_{13}^+ were fit to describe the electrostatic potential on a grid of points around molecules, as well as molecular gas phase dipole moment, all obtained from QC calculations at MP2/aug-cc-pvDz level for cations and MP2/cc-pvTz for TFSI. Second, bond lengths and natural bending angles were taken from APPLE&P without modification. Third, dihedral angle parameters were determined by fitting the gas phase conformational-energy surface of model molecules as determined from quantum chemistry as previously described for APPLE&P.[1a] Fourth, the repulsion-dispersion parameters (see Table S1) were developed. The $C_U\ldots C_U$ and $C_{mU}\ldots C_{mU}$ repulsion-dispersion parameters were fit to density and heat of vaporization of C_5H_{12} and $C_{10}H_{22}$ as shown in Table S2. Next, $C_N\ldots C_N$ and $C_{mN}\ldots C_{mN}$ repulsion-dispersion parameters were fit to $[pyr_{13}][TFSI]$ and $[N_{4111}][TFSI]$ density and self-diffusion coefficient from experiments and heats of vaporization obtained from MD simulations using APPLE&P force field as shown in Table S2. The TFSI S…S repulsion-dispersion interactions were adjusted to improve ion self-diffusion coefficients of $[pyr_{13}][TFSI]$, $[pyr_{14}][TFSI]$ and $[N_{4111}][TFSI]$ as a function of temperature shown in Figure S5 and S6. We could not simultaneously obtain a good fit for ion self-diffusion coefficient and heat of vaporization, therefore, we settle of the compromise when MD simulations using UA force field yielded ion-self diffusion coefficients lower than experiments and MD simulations using APPLE&P data, while heat of vaporization was slightly below the results of MD simulations with APPLE&P.

Comparison of Nonpolarizable United Atom and All Aton Polarizable Models

We begin comparison of the nonpolarizable UA and polarizable AA (APPLE&P) force fields by analyzing n-alkane data shown in Table S2. We observe that for the same density and heat of vaporization UA model predicts faster by 16% and 67% self-diffusion coefficients for C_5H_{12} and $C_{10}H_{22}$, respectively. Note that MD simulations using UA models using Lennard-Jones 12-6 repulsion-dispersion form predicted $C_{10}H_{22}$ self-diffusion coefficient only 10% faster than experiments.[7] The slower diffusion for the Lennard-Jones 12-6 UA model compared to the currently used exp-6 is attributed to the steeper repulsive part of the former functional form. We could have increased the λ steepness parameter beyond values of 14-16, typically used in APPLE&P force field, thus, decreasing the self-diffusion coefficient for *n*-alkanes and brining them close to the experimental values. We, however, have not done this because at high λ of >20 ion diffusion in ILs would significantly decrease deteriorating description of IL transport properties.

Comparison of density, heat of vaporization and ion self-diffusion coefficients from MD simulations using UA model and APPLE&P show is shown in Table S3. The UA model was successfully fit to match experimental and APPLE&P densities, while we could not describe ion self-diffusion coefficients as a function of temperature. At high temperature (393 K) agreement between MD simulations using UA force field and experiments is generally good, with MD simulations with UA force field predicting self-diffusion coefficients 8-38% lower. In the simulations reported here no finite size correction to ion self-diffusion coefficients was applied because IL viscosity needed for calculating this correction was calculated.[1a] Magnitude of the finite size correction is expected to be around 10% for the simulated ILs and box sizes. Application of this correction will reduce the disagreement between MD simulations using UA force field and extrapolated experimental data to below 28% at 393 K. As temperature decreases to 298 K description of the ion self-diffusion coefficient from MD simulations using UA force field deteriorates and we observed a disagreement of a factor of 2-4 with experiments and the results using APPLE&P force field as shown in Figures S5 and S6. Note that MD simulations using APPLE&P force field yielded ion transport in excellent agreement with experiments.[1a] Higher activation energy for the diffusion coefficient temperature dependence of the UA nonpolarizable force field vs. polarizable AA (APPLE&P) force field is attributed to the absence of polarization in the UA force field as previously discussed.[1a, 8] Despite the deficiency of UA nonpolarizable force field in describing temperature dependence of ion dynamics, we feel that the developed force field is an significant improvement over the previous publications for alkylpyrrolidinium and alkylammonium-based ILs. Indeed, Tsuzuki et al.[9] predicted ion diffusion of $[N_{4111}][TFSI]$ and $[pyr_{14}][TFSI]$ a factor of 20-40 slower than experiments at 353 K. Siqueira et al.[10] predicted ion diffusion of [*N*-ethyl-*N*,*N*-dimethyl-*N*-(2-methoxyethyl)ammonium][TFSI] about 1 order of magnitude lower than experiments.

Ability of the developed UA force field to describe ionic liquid structure was investigated by comparing the three dimensional (3-D) distribution function of the $TFSI^-$ oxygen atom (denoted O(TFSI)) around pyr_{13}^+ and N_{4111}^+ cation shown in Figure S7 and S8, respectively, and the center of mass radial distribution functions (RDF's) shown in Figure S9. We observe that the isosurfaces of O(TFSI) around pyr_{13}^+ are slightly shifted and occupy a significantly larger space. This behavior is consistent with the maximum of the 3-D distribution first peak being 56 for UA model and only 35 for APPLE&P. A significantly higher first maximum of 3-D distribution and larger occupied space for the isosurface are indicative of a stronger ordering of pyr_{13}^+ and $TFSI^-$ in a liquid phase for UA model compared to AA model resulting is a slower dynamics for the former model. Somewhat similar picture was observed for $[N_{4111}][TFSI]$, with the maximum of 3-D distribution first peak being 47 for UA and 15 for AA

APPLE&P, however, a larger discrepancy of 3-D isosurfaces was observed for [N_{4111}][TFSI] compared to [pyr_{13}][TFSI].

The center of mass RDFs shown in Figure S9 indicate that UA model describes the TFSI-TFSI center of mass in excellent agreement with APPLE&P, while a noticeable difference is observed for the first peak of pyr_{13}-TFSI and pyr_{13}-pyr_{13} RDF obtained from MD simulations using UA and APPLE&P force field. Note, however, that the radial structure of the pyr_{13}-TFSI and pyr_{13}-pyr_{13} is in excellent agreement between UA model and APPLE&P. Finally, heat of vaporization of the UA model was found to be somewhat lower than for APPLE&P as shown in Table S3.

We conclude that the developed efficient nonpolarizable united atom force field adequately predicts ionic liquid density, heat of vaporization, structure and dynamics.

Appendix

Molecular Dynamics Simulation Details

A version of the MD simulation package *Lucretius* that includes many-body polarization was used for all MD simulations.[11] A three-dimensional, periodic cubic simulation cell consisted of 150 ion pairs of $[N_{4111}][TFSI]$, $[pyr_{14}][TFSI]$ and 216 ion pairs of $[pyr_{13}][TFSI]$ was simulated, while C_5H_{12} and $C_{10}H_{22}$ simulation cells consisted of 216 and 125 molecules, respectively. The IL initial configurations were created in the gas phase corresponding to a cell (linear) dimension of approximately 90-110 Å. The dimensions of the simulation cells were reduced to yield estimated densities at 393 K followed by 1 ns NPT runs. The Ewald summation method was used for electrostatic interactions between partial charges with partial charges and partial charges with induced dipole moments using k^3 from 7^3 to 8^3 k-vectors, and α from 9 - 9.5 Å for ionic liquids. The C_5H_{12} and $C_{10}H_{22}$ UA force field had zero partial charges, therefore, no Ewald summation was used. Multiple timestep integration with an inner timestep of 0.5 fs (bonded interactions), a central time step of 1.5 fs for all nonbonded interactions within a truncation of 7.0 Å and an outer timestep of 3.0 fs for all nonbonded between 7.0 Å and the nonbonded truncation distance of 10.5 or 11 Å as well as for the reciprocal part of Ewald was employed. A Nose-Hoover thermostat (NPT and NVT simulations) and a barostat (NPT simulations) were used to control the temperature and pressure with the associated frequencies of 10^{-2} and $0.5x10^{-3}$ fs. Induced dipoles were calculated via a direct iteration with a predictor method. Brownian dynamics simulations of ion pairs were performed at 298 K for 2-4 ns to yield gas phase ion pair energies. The number of simulated ion pairs was the same as in the simulation box used for simulating the liquid phase.

Table 1. The repulsion-dispersion (R/D) types and a list of compounds and properties[a] used for their fitting.

Label	atom R/D types
C_U	sp^3 carbon in - CH_2 - group
C_{mU}	sp^3 carbon at chain ends (CH_3-, CF_3- groups) not connected to N^+
C_m	sp^3 carbon at chain ends (CF_3- groups), fluorine atoms were not callapsed
C_N	sp^3 carbon in - CH_2 - group connected to N^+
C_{Nm}	sp^3 carbon at chain ends (CH_3-, CF_3- groups) connected to N^+
N^+	nitrogen with the formal charge +1e
O=	all oxygen atoms (O=S)
F	all fluorine atoms
S^-	sulfur in $TFSI^-$

Table S2. Thermodynamic properties (density, heat of vaporization, self-diffusion coefficient) of n-alkanes from MD simulations (ρ^{MD}, H_{vap}^{MD}, D^{MD}) using united atom force field, experiments (ρ^{exp}, H_{vap}^{exp}, D^{exp}) and deviation of MD results from experiments ($\Delta\rho$,ΔH_{vap}, ΔD) in per cents.

Liquid	ρ^{MD} (ρ^{exp}) **$\Delta\rho$(%)** (kg m^{-3})	H_{vap}^{MD} (H_{vap}^{exp}) **ΔH_{vap}(%)** (kJ/mol)	D^{MD} (D^{exp}) **ΔD(%)** (10^{-10} m^2/s)	references
C_5H1_2	628 (621) **1.1**	26.7 (26.7) **-0.3**	65.5 (56.2) **17**	12,12,13
$C_{10}H_{22}$	726.7 (724.7) **0.3**	51.9 (51.4) **0.9**	22.7 (14) **62**	12, 12,7

Table S3. Thermodynamic properties of ionic liquids from MD simulations (ρ^{MD}, H_{vap}^{UA}, D^{MD}) using united atom force field, all atom force field H_{vap}^{UA}, experiments (ρ^{exp}, D^{exp}).

	T (K)	ρ^{MD} (ρ^{exp}) (kg m^{-3})	H_{vap}^{UA} (H_{vap}^{AA}) (kJ/mol)	D_+^{MD} (D_+^{exp}) (10^{-10} m^2/s)	D_-^{MD} (D_-^{exp}) (10^{-10} m^2/s)	references
$[N_{4111}][TFSI]$	393	1325		1.36 (2.22)	1.36 (2.07)	
$[N_{4111}][TFSI]$	333	1373 (1357)		0.20 (0.538)	0.21 (0.487)	14
$[N_{4111}][TFSI]$	298	1406 (1393)	145.9 (157.1)	0.031 (0.131)	0.035 (0.117)	14
$[pyr_{13}][TFSI]$	393	1341 (1343)		2.2	2.0	14-15
$[pyr_{13}][TFSI]$	333	394 (1384)		0.43	0.42	15
$[pyr_{13}][TFSI]$	298	1426 (1408-1447)	140.0 (143.6)	0.086 (0.26)	0.085 (0.17)	15a
$[pyr_{14}][TFSI]$	393	1297		1.6 (2.3)	1.9 (2.1)	14
$[pyr_{14}][TFSI]$	333	1353 (1367)		0.29 (0.64)	0.33 (0.53)	14
$[pyr_{14}][TFSI]$	298	1384 (1399)	143.2 (147.6)	0.038 (0.177)	0.051 (0.142)	14

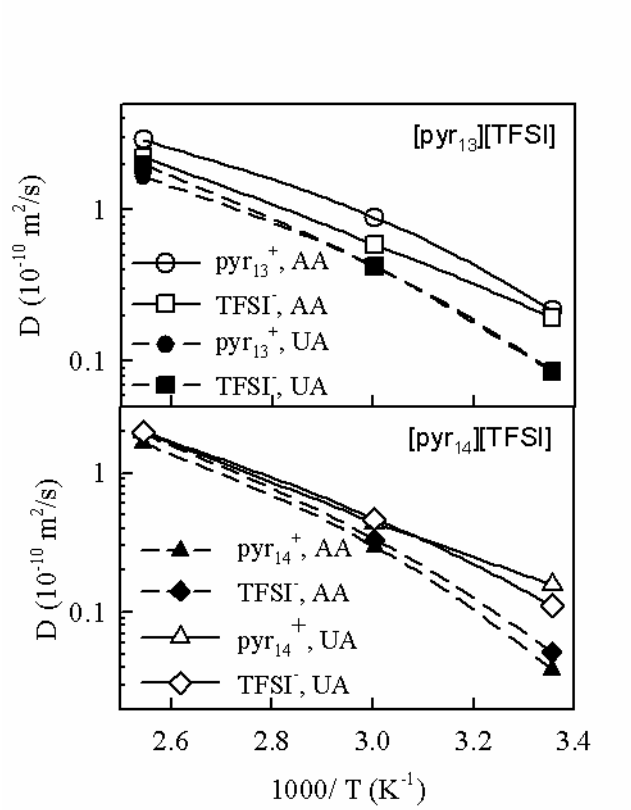

Figure S5. Ion self-diffusion coefficients from MD simulations of $[pyr_{13}][TFSI]$ and $[pyr_{14}][TFSI]$ using nonpolarizable UA and AA APPLE&P force field.

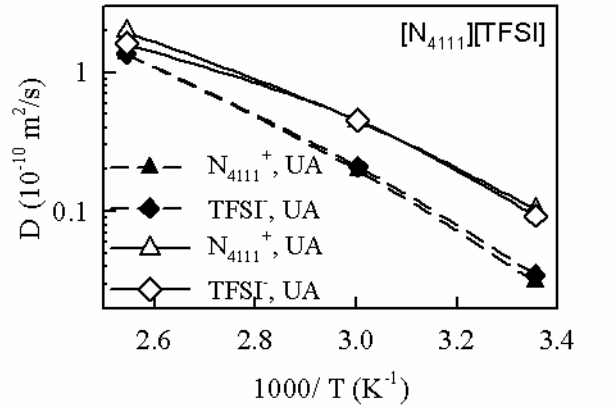

Figure S6. Ion self-diffusion coefficients from MD simulations of $[N_{4111}][TFSI]$ and $[pyr_{14}][TFSI]$ using nonpolarizable UA and AA APPLE&P force fields.

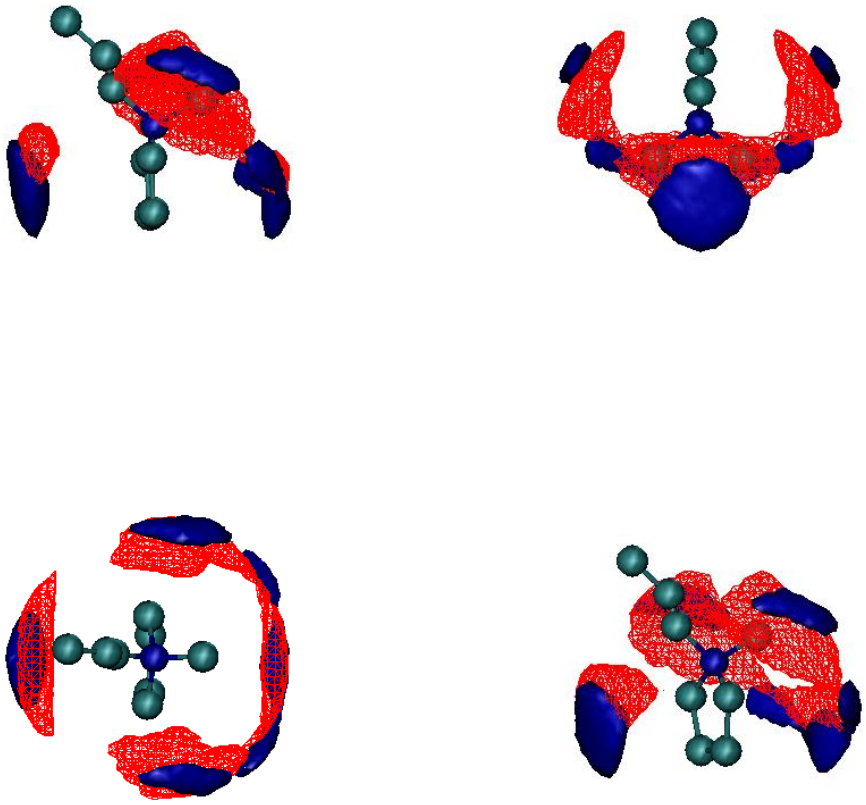

Figure S7. Isosurface of oxygen of $TFSI^-$ around pyr_{13}^+ cation for $\rho/\rho^{random}=7$ (ρ-local number density), where red wireframe isosurface for UA force field, blue solid isosurface for APPLE&P force field.

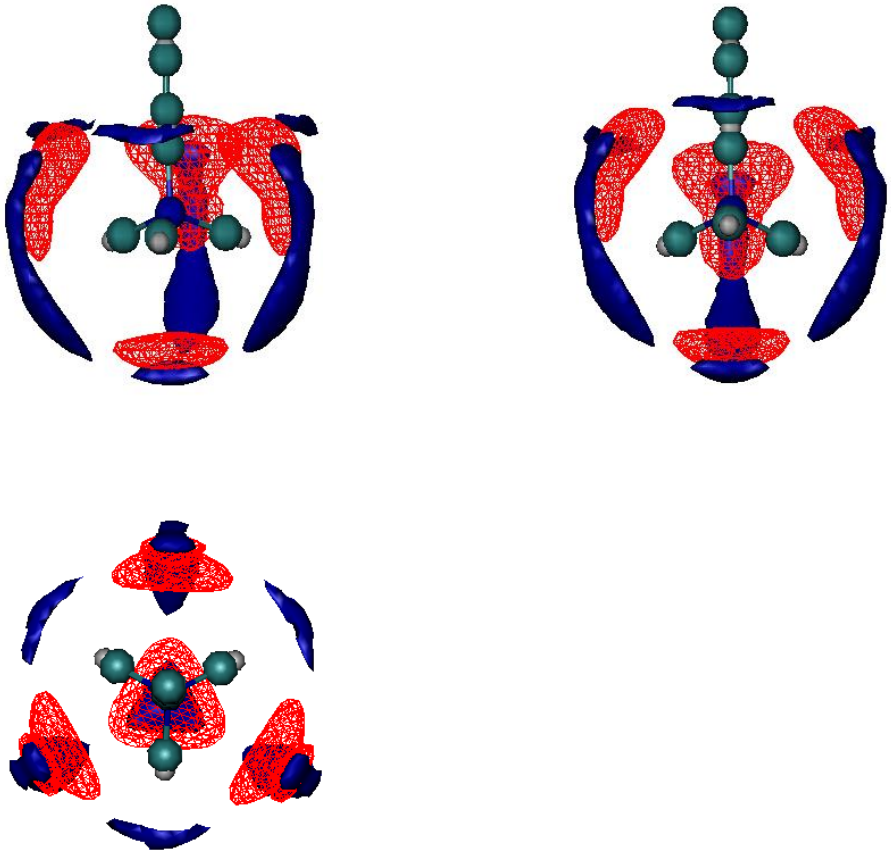

Figure S8. Isosurface of oxygen of $TFSI^-$ around $N4111^+$ cation for $\rho/\rho^{random}=8$ (ρ-local number density), where red wireframe isosurface for UA force field, blue solid isosurface for APPLE&P force field.

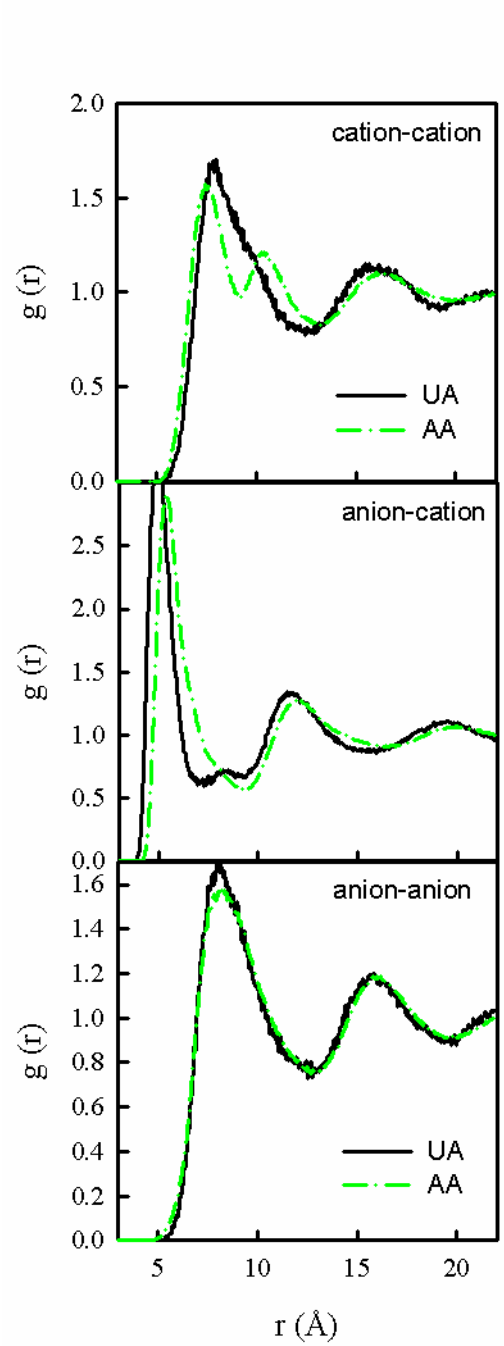

Figure S9. Center of mass radial distribution functions (RDFs) from MD simulations of [pyr_{13}][TFSI] using nonpolarizable UA and AA APPLE&P force fields.

References

1. (a) Borodin, O., Polarizable Force Field Development and Molecular Dynamics Simulations of Ionic Liquids. *J. Phys. Chem. B* **2009,** *113*, 11463-11478; (b) Borodin, O.; Gorecki, W.; Smith, G. D.; Armand, M., Molecular Dynamics Simulation and Pulsed-Field Gradient NMR Studies of Bis(fluorosulfonyl)imide (FSI) and Bis[(trifluoromethyl)sulfonyl]imide (TFSI)-Based Ionic Liquids. *J. Phys. Chem. B* **2010,** *ASAP, 10.1021/jp911950q*.

2. Borodin, O.; Smith, G. D., Development of Many-Body Polarizable Force Fields for Li-Battery Components: 1. Ether, Alkane, and Carbonate-Based Solvents. *J. Phys. Chem. B* **2006,** *110*, 6279-6292.
3. Pierce, F.; Tsige, M.; Borodin, O.; Perahia, D.; Grest, G. S., Interfacial properties of semifluorinated alkane diblock copolymers. *J. Chem. Phys.* **2008,** *128*, 214903-14.
4. Borodin, O.; Smith, G. D., Development of Many-Body Polarizable Force Fields for Li-Battery Applications: 2. LiTFSI-Doped Oligoether, Polyether, and Carbonate-Based Electrolytes. *J. Phys. Chem. B* **2006,** *110*, 6293-6299.
5. (a) Borodin, O.; Smith, G. D., Structure and Dynamics of (*N*-Methyl-*N*-Propylpyrrolidinium)$^{+}$(TFSI)$^{-}$ Ionic Liquid From Molecular Dynamics Simulations. *J. Phys. Chem. B* **2006,** *110*, 11481-11490; (b) Borodin, O.; Smith, G. D.; Fan, P., Molecular Dynamics Simulations of Lithium Alkyl Carbonates. *J. Phys. Chem. B* **2006,** *110*, 22773-22779; (c) Borodin, O.; Smith, G. D.; Geiculescu, O.; Creager, S. E.; Hallac, B.; DesMarteau, D., Li^{+} Transport in Lithium Sulfonylimide-Oligo(ethylene oxide) Ionic Liquids and Oligo(ethylene oxide) Doped with LiTFSI. *J. Phys. Chem. B* **2006,** *110*, 24266-24274; (d) Borodin, O.; Smith, G. D.; Henderson, W., Li^{+} Cation Environment, Transport and Mechanical Properties of the LiTFSI Doped *N*-Methyl-*N*-Alkylpyrrolidinium^{+}TFSI^{-} Ionic Liquids. *J. Phys. Chem. B* **2006,** *110*, 16879 -16886.
6. McCabe, C.; Bedrov, D.; Borodin, O.; Smith, G. D.; Cummings, P. T., Transport properties of perfluoroalkanes using molecular dynamics simulation: Comparison of united- and explicit-atom models *Ind. & Eng. Chem. Res.* **2003,** *42*, 6956-6961.
7. Mondello, M.; Grest, G. S., Viscosity calculations of n-alkanes by equilibrium molecular dynamics. *Journal of Chemical Physics* **1997,** *106*, 9327-9336.
8. Bedrov, D.; Borodin, O.; Li, Z.; Smith, G. D., Influence of Polarization on Structural, Thermodynamic, and Dynamic Properties of Ionic Liquids Obtained from Molecular Dynamics Simulations. *J. Phys. Chem. B* **2010,** *114*, 4984-4997.
9. Tsuzuki, S.; Shinoda, W.; Saito, H.; Mikami, M.; Tokuda, H.; Watanabe, M., Molecular Dynamics Simulations of Ionic Liquids: Cation and Anion Dependence of Self-Diffusion Coefficients of Ions. *J. Phys. Chem. B* **2009,** *113*, 10641-10649.
10. Siqueira, L. J. A.; Ribeiro, M. C. C., Molecular dynamics simulation of the ionic liquid N-Ethyl-N,N-dimethyl-N-(2-methoxyethyl)ammonium bis(trifluoromethanesulfonyl)imide. *Journal of Physical Chemistry B* **2007,** *111*, 11776-11785.
11. Ayyagari, C.; Bedrov, D.; Borodin, O.; Smith, G. D. Lucretius, MD simulation code http://www.eng.utah.edu/~gdsmith/lucretius.html.
12. http://webbook.nist.gov/chemistry/, NIST Webbook.
13. Fishman, E., Self-Diffusion in Liquid Normal Pentane and Normal Heptane. *J. Phys. Chem.* **1955,** *59*, 469-472.
14. Tokuda, H.; Ishii, K.; Susan, M. A. B. H.; Tsuzuki, S.; Hayamizu, K.; Watanabe, M., Physicochemical properties and structures of room-temperature ionic liquids. 3. Variation of cationic structures *J. Phys. Chem. B* **2006,** *110*, 2833-2839.
15. (a) Nicotera, I.; Oliviero, C.; Henderson, W. A.; Appetecchi, G. B.; Passerini, S., NMR investigation of ionic liquid-LiX mixtures: Pyrrolidinium cations and TFSI- anions. *J Phys Chem B* **2005,** *109*, 22814-22819; (b) MacFarlane, D. R.; Meakin, P.; Sun, J.; Amini, N.; Forsyth, M., Pyrrolidinium imides: A new family of molten salts and conductive plastic crystal phases. *J. Phys. Chem. B* **1999,** *103*, 4164-4170